A Power Quality Prediction System

Steven R. Shaw, *Student Member, IEEE*, Chris R. Laughman, Steven B. Leeb, *Member, IEEE*, and Rob F. Lepard

***Abstract*—This paper describes two hardware prototypes and estimation schemes for determining the parameters of a simple, physically based, point-of-use electric utility model using transient measurements. Parameters of the utility model are estimated using data collected by the prototypes. Frequency-dependent effects observed in previous work in this area are modeled. Performance of the techniques given is demonstrated by comparison of measured and predicted line voltage distortion during current transients created by several loads.**

***Index Terms*—Estimation, power distribution testing, prediction methods.**

I. Background

FROM A SERVICE outlet, the electrical utility can be approximated as a sinusoidal voltage source in series with an inductor and a resistor. In a commercial or industrial building, impedances seen at the "user interface" arise predominantly from an upstream transformer, protection circuitry, and cabling. Harmonic currents generated by loads flow through these impedances, creating voltage drops that result in a distorted voltage waveform at the service outlet.

In [1], an interesting technique for determining the local apparent impedance of the electrical utility service is presented. The impedance is identified by briefly closing a capacitor across the electrical service at a precise point in the line voltage waveform. The shape and decay of the transient current in the resulting *RLC* circuit can be used to estimate the line impedance.

In this paper, the technique in [1] is reformulated in two point-of-load impedance characterization and voltage distortion prediction systems. The first system (method A) uses the *RLC* transient excitation technique from [1], but features a digitally programmable test capacitor, a phase-programmable switch, and a data collection interface. The second system (method B) consists of a programmable current source, providing more flexibility in test transients. The two systems, and their associated estimation procedures, share a point-of-load model of the electric utility. This model, motivated by theory, accounts for the measured increase in resistance as a function of test transient frequency observed in [1] and [2]. Ultimately, the model and estimated parameters are used to predict voltage distortion from transient currents.

Manuscript received February 16, 1998; revised November 25, 1999. Abstract published on the Internet March 12, 2000. This work was supported by the Office of Research and Development, a CAREER Award from the National Science Foundation, and the Carl Richard Soderberg Career Development Chair, Massachusetts Institute of Technology.

S. R. Shaw, C. Laughman, and S. B. Leeb are with the Laboratory for Electromagnetic and Electronic Systems, Massachusetts Institute of Technology, Cambridge, MA 02139 USA.

R. Lepard is with the Aeronautical Systems Command, U.S. Air Force, Wright-Patterson Air Force Base, Dayton, OH USA.

Publisher Item Identifier S 0278-0046(00)04738-9.

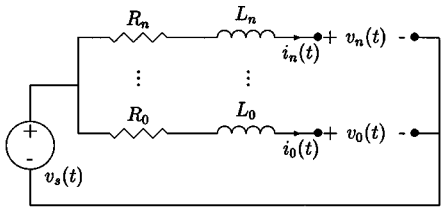

Fig. 1. A distribution-level model of the electric utility.

We begin with the common utility model and comparison of the excitation hardware for test methods A and B. The system identification procedures corresponding to each method are then discussed in separate sections. Juxtaposition of the methods resumes in Sections VI and VII, which include demonstrations of the techniques on measured data and observations regarding applications beyond the laboratory.

II. Utility Model and Measurements

For the purpose of point-of-load voltage distortion prediction, we consider a single-phase line-to-neutral connection to the electric utility, e.g., v_0 in Fig. 1. Electrical loads are connected to a source $v_s(t)$ through lumped parameters R and L modeling physical cabling, protection devices, and other impedances. The source $v_s(t)$ is stiff with respect to the current drawn from any particular load, but may have distortion resulting from the aggregate load current. Physically, for example, v_s might correspond to the voltage on the bus bars of a breaker cabinet. The voltage across these bus bars might be shaped by power-factor-correction capacitors, upstream voltage distortion, and the aggregate current drawn by the loads. However, to continue the physical example, we assume that the voltage on the bus bars is essentially invariant to current perturbations on the order of the currents drawn by the *individual* loads. A similar model is used in [1] and [2].

Consider the kth connection to the model shown in Fig. 1. Assuming measurements $v_k(t)$, $v_s(t)$, and $i_k(t)$ are available, the parameters R_k and L_k of the utility model can be estimated. The quantity $v_s(t)$ is generally inaccessible and difficult to measure. However, following the assumption that $v_s(t)$ is stiff and if most loads are in steady state

$$v_s(t) \approx v_s(t - nT) \tag{1}$$

for small multiples n of the fundamental period T. Using this assumption, measurements $v_k(t - nT)$ with $i_k(t - nT) = 0$ could approximate $v_s(t)$ when $i_k(t) \neq 0$. That is, the estimate

$$\hat{v}_s(t) = v_k(t - nT), \quad \text{with } i_k(t - nT) = 0. \tag{2}$$

As an experimental procedure, one could simply measure several periods of $v_k(t)$ before and while applying the test load.

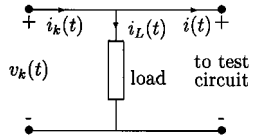

Fig. 2. Steady-state currents i_L in measurement scenario.

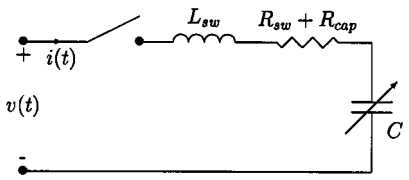

(a)

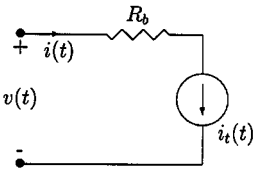

(b)

Fig. 3. Test circuits used to excite utility for identification. Test circuit *A* is a programmable capacitor connected to the utility by a switch. Test circuit *B* is a programmable current source. The voltage $v(t)$ and current $i(t)$ are measured during transient excitation.

The notion of a test during steady-state conditions can be extended to include an unmeasured steady-state load current $i_L(t) = i_L(t - nT)$ if there is a linear operator H relating $v_s(t) - v_k(t)$ to $i_k(t)$. Let the quantities $i(t)$, $v(t)$ be the actual measurements as made by the test apparatus shown in Fig. 3 and discussed in the next section. In the absence of i_L, the equation

$$Hi(t) = \hat{v}_s(t) - v(t) \tag{3}$$

is used to estimate the parameters. If the unmeasured load current i_L is introduced at the test node k so that

$$i_k(t) = i(t) + i_L(t) \tag{4}$$

as indicated in Fig. 2, then (2) becomes

$$\hat{v}_s(t) = v_k(t - nT), \quad \text{with } i_k(t - nT) = i_L(t - nT). \tag{5}$$

The effect is to introduce terms Hi_L in the right-hand side of (3) that cancel if $i_L(t)$ is steady state

$$\begin{aligned} Hi(t) &= \hat{v}_s(t) - v(t) \\ &= (v_s(t - nT) - Hi_L(t - nT)) \\ &\quad - (v_s(t) - H(i_L(t) + i(t))). \end{aligned} \tag{6}$$

A steady-state load current $i_L(t) = i_L(t - nT)$ therefore has no effect on the problem. In some cases, $i_L(t)$ might be perturbed dramatically during the test, for example, if a load connected to the point of test is essentially a capacitor. In this case, the problematic load should be disconnected during the test. In principle, provided sufficient excitation can be maintained, interacting loads may remain connected if the current measurement is modified to include i_L.

The model Fig. 1 is accurate in the sinusoidal steady state at a particular frequency. Over the frequencies that we considered, in particular, from the fundamental at 60 Hz to around the 16th harmonic, skin and proximity effects in the physical system require the resistors R_k to be nonlinear, increasing functions of frequency. The two hardware prototypes and their associated identification procedures, discussed in the subsequent sections, handle this frequency dependence slightly differently.

III. Prototype Hardware

Numerical values of the utility model parameters are needed to predict the effects of currents on the voltage waveform at the load. To find parameter values, it is necessary to excite the utility at the point of load with some test circuit, measure the response, and determine the parameters. Two excitation circuits, shown in Fig. 3, were considered for this paper.

The principle components in Fig. 3(a) are the capacitor and the switch. When the switch closes, the capacitor "rings" with the R and L of the utility model in Fig. 1, creating the excitation. The firing angle of the switch is programmable with a resolution of 10 b, i.e., a resolution of one part in 1024 parts of a line cycle. The time reference subdividing each line cycle is obtained from a phase-locked loop. Similarly, the capacitor value is selectable with a resolution of 7 b by selectively engaging a parallel array of seven capacitors C_n with $C_{k+1} = 2C_k$. The programmability of the switch firing angle and capacitor value allows rapid collection of a set of transient frequencies and may be used to create tests that draw reasonable currents for a range of source voltages. Also shown in Fig. 3(a) are parasitic inductance $L_{\rm sw}$ and resistance $R_{\rm sw} + R_{\rm cap}$, which may change depending on the configuration of the switch. The choice of measurements $v(t)$ and $i(t)$ makes the specific values of the parasitics unimportant. Identification and prediction procedures associated with the circuit in Fig. 3(a) will be called "method A."

The test circuit in Fig. 3(b) consists of a MOSFET current sink and ballast resistor R_b. The MOSFET is operated linearly and dissipates power during an individual test, but subsequent tests can be spaced in time to keep the average power dissipation in the MOSFET within specifications. The noncritical ballast resistor R_b can also be sized to keep power dissipation in the MOSFET reasonable for a range of nominal source voltages. Procedures associated with Fig. 3(b) will be collectively called "method B."

IV. Estimation and Prediction for Method A

The procedure for method A is to probe the utility at several different frequencies using the test circuit of Fig. 3(a) and estimate values of R and L for each frequency. Experimentally, as in [1], the estimates are found to depend on frequency. In this section, we extend the model of Fig. 1 with a correction for the frequency dependence and show how the aggregate model can be used to predict voltage distortion.

A. Identification of the Parameters R and L

The parameters R and L form the constraint

$$v_s(t) - v(t) = (R + Lp)i(t). \tag{7}$$

where p is the operator d/dt. The parameters R and L could be found directly from (7) if $pi(t)$, $i(t)$, and $v_s(t) - v(t)$ were available. The data, however, consist of samples $i(nT_s)$, $v(nT_s)$, and $\hat{v}_s(nT_s)$, where T_s is the sampling period and $\hat{v}_s$ is the estimate of the source voltage as in Section II.

We eliminate problems associated with measuring or approximating the derivatives in (7) via the low-pass operator

$$\lambda = \frac{1}{1 + p\tau} \tag{8}$$

with $\tau > 0$ [8]. With some manipulation

$$p = \frac{1 - \lambda}{\lambda\tau} \tag{9}$$

where λ is an *operator*, i.e., λx is the result of applying the low-pass filter (8) to x. By substituting $\hat{v}_s(t)$ and p and multiplying through by $\lambda\tau$, (7) becomes

$$\tau\lambda(\hat{v}_s(t) - v(t)) = (R\tau\lambda + L(1 - \lambda))i(t). \tag{10}$$

There is no derivative in this equation, and the only difficulty is to compute λ applied to measured quantities. Equation (10) can be rewritten to produce a linear least-squares tableau

$$\tau\lambda\begin{pmatrix} (\hat{v}_s - v) & -i \end{pmatrix}\begin{pmatrix} \hat{\beta}_1 \\ \hat{\beta}_2 \end{pmatrix} = (1 - \lambda)i \tag{11}$$

where $\hat{\beta}_1$, $\hat{\beta}_2$ are estimates of $1/L$, R/L. Quantities i, v, and $\hat{v}_s$ are columns vectors of samples, so that $(\hat{v}_s - v \;\; -i)$ is a two-column by N matrix, where N is the number of samples. The operator λ acts on the matrix in (11), hence, the regressors are low-pass. Unless disturbances are also pathologically low-pass, for large N the estimates will be unbiased. A detailed noise model for this method can be found in [8].

The time constant τ associated with λ must be determined by the user. The time constant should be chosen to preserve information content and minimize disturbances. The results presented in Section VI-A were obtained with $\tau = .002$ s; in practice, a relatively wide range of values of τ produces satisfactory estimates. Although λ is a continuous-time operator, we have found that it can be applied offline to linear or zero-order-hold interpolations of the finely sampled quantities with little error. Discrete-time implementation of λ may be desirable in some circumstances.

B. Estimating Transient Frequency

In [1], estimates of R and L at different transient frequencies uncovered a frequency dependence in R. To explore and model this frequency dependence, an accurate means of estimating the principle transient frequency is required.

The frequency of the *RLC* transient is

$$f = \frac{1}{2\pi}\sqrt{\frac{1}{L_t C} - \frac{R_t^2}{4L_t^2}} \tag{12}$$

where $R_t = R_p + R$, $L_t = L_p + L$, and L_p and R_p appear in Fig. 3(a). One approach to find $\hat{f}$ is to determine the parameters R_t, L_t, and C and apply (12). Over short intervals, this technique is preferable to timing zero crossings because it is relatively insensitive to noise at the zero crossings and is independent of the steady-state response at the line frequency.

To find estimates $\hat{R}_t$, $\hat{L}_t$, and $\hat{C}$, we apply the λ-operator technique to the equation relating $i(t)$ to $v_s(t)$ in Fig. 3

$$v_s(t) = \left(R_t + L_t p + \frac{1}{Cp}\right) i(t). \tag{13}$$

Substituting $\hat{v}_s$ and p yields

$$\tau\lambda\begin{pmatrix} (1 - \lambda)i & \tau\lambda i & (\lambda - 1)\hat{v}_s \end{pmatrix}\begin{pmatrix} \hat{\alpha_1} \\ \hat{\alpha_2} \\ \hat{\alpha_3} \end{pmatrix} = (-1 + 2\lambda - \lambda^2)i \tag{14}$$

where $\hat{\alpha_1}$, $\hat{\alpha_2}$, and $\hat{\alpha_3}$ are estimates of R_t/L_t, L_t/C, and $1/L_t$, respectively. Equation (14) is solved in the least-squares sense and the parameter estimates are used to compute the transient frequency f using (12).

C. Frequency Dependence of R

In [1] and in the experiments in our laboratory, the estimated resistances $\hat{R}$ were observed to be an increasing function of the frequency f of the transient. Phenomena that could explain this observation include, for example, skin effect in the wires and eddy currents induced in conductors adjacent to the wires.

In [9], the change of resistance due to the skin effect in a conductor with cylindrical geometry is given for $x \ll 1$ ("low" frequencies) as

$$\frac{R}{R_0} \approx 1 + \frac{x^4}{192} \tag{15}$$

where $x \propto \sqrt{f}$ and the constant of proportionality, given explicitly in [9], is related to the physical properties and geometry of the conductor. The variable R_0 is the dc resistance.

From [9], eddy currents in conductive materials adjacent to current-carrying wires produce changes in effective resistance as in (16), which is valid for $\theta \ll 1$

$$R \approx R_0 + 2\pi f L_0 \frac{\theta^2}{6}. \tag{16}$$

Here, $\theta \propto \sqrt{f}$. Again, the constant of proportionality is geometry and material dependent, and can be found analytically for certain geometries.

Assuming that the constants relating x and θ to $\sqrt{f}$ are favorably scaled, (15) and (16) suggest the following fitting function, with parameters R_0 and δ:

$$R(f) = R_0 + \delta f^2. \tag{17}$$

With several estimates $\hat{R}(f)$ made at different frequencies, a least-squares solution for the parameters $\hat{R}_0$ and $\hat{\delta}$ can be found which satisfies (17). Transient tests at different frequencies can be automatically conducted by the system simply by programming a range of values for C. It may be possible, based on the value of δ, to determine frequencies above which (17) becomes

invalid. However, this was not investigated in detail here because the purpose is to extrapolate the data to *lower* frequencies, and because the collected data at higher frequencies are well interpolated by (17). Equations (15) and (16) apply to the sinusoidal steady state. However, for conventional materials, the important time constants are sufficiently short that the application of these equations to our test transients is a good approximation.

D. Power Quality Prediction

With estimates $\hat{L}_0$, $\hat{R}_0$, and $\hat{\delta}$, we would like to predict the distorted voltage $\hat{v}(t)$ due to some measured or known current $i(t)$. Fortunately, the nonlinear dependence of the resistance as a function of transient frequency (17) can be interpreted in terms of a linear transfer characteristic

$$\frac{V_s(s) - V(s)}{I(s)} = R_0 + Ls - \delta s^2. \tag{18}$$

Equation (18) could also be used for identification of the parameters using a regression matrix composed of several transient measurements. However, it is necessary to ensure by inspection of the data that the approximations inherent in (17) are valid on a case-by-case basis. It is more straightforward to perform this check by performing a "two-step" regression rather than a "one-step" regression. Using a finite-difference approximation of the derivative, (18) can be used to simulate the distorted voltage waveform estimate $\hat{v}(t)$ given a parameter set and $v_s(t)$, $i(t)$.

V. Estimation and Prediction for Method B

In addition to using excitation hardware different from method A, a different identification and prediction procedure was explored for method B. There are two principle advantages of the method B identification procedure. First, since the current source in Fig. 3(b) can produce a wide variety of test waveforms relative to the possibilities offered by Fig. 3(a), the two-step identification procedure of method A is replaced with a one-step procedure. With method B, test currents can have whatever frequency content is useful. Second, the model identified by method B is a discrete-time model. While the continuous time parameters are interesting, identification and voltage distortion prediction is done in a sampled data environment where a discrete-time model facilitates both tasks.

A. Measurement Preprocessing

One of the difficulties experienced with method B, particularly when testing with a relatively stiff wall, was quantization error. When measuring the voltage, the undistorted part of the waveform required most of the range of the A/D converter, leaving only a few bits for the distortion due to the test current. To remedy this problem, a high-pass preprocessing filter

$$G(s) = \frac{\alpha s}{\alpha s + 1} \tag{19}$$

was used prior to A/D conversion. The preprocessing filter reduces the magnitude of the 60-Hz component of the voltage waveform so that it is comparable to the higher frequency distortion created by the test excitation. Measuring $Gv(t)$ rather than $v(t)$ has the effect of capturing the interesting parts of voltage waveform with more bits.

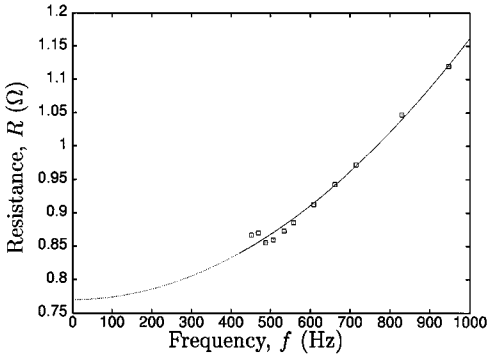

Fig. 4. Resistance R as a function of frequency f, for method A. Solid line shows model fit in the region of support of the measurements; dashed line is the extrapolation to lower frequencies.

Measurement preprocessing can be done without affecting the system identification procedure, provided that sufficient excitation remains in the preprocessed signals and that the system to be identified commutes with the preprocessing operator. Ordinarily, parameters of the operator H

$$y(t) = Hx(t) \tag{20}$$

are identified from the input/output signals $x(t)$, $y(t)$. If H commutes with a preprocessing operator G, then

$$Gy(t) = HGx(t) \tag{21}$$

and preprocessed input/output variables $Gy(t)$ and $Gx(t)$ can be used for identification in the same way that the original variables were used in (20). The parameters of G, i.e., α in (19), are unimportant as long as the operator preserves the excitation. The requirement that H and G commute is satisfied if both are linear differential operators.

B. Discrete-Time Model and Identification

The continuous-time model, including the frequency dependence of R, can be written

$$v_s(t) - v(t) = (R + Lp + \delta p^2)i(t). \tag{22}$$

The behavior of (22) can be captured by a discrete-time approximation, for example,

$$P_a^2(z^{-1})(v_s[k] - v[k]) = P_b^2(z^{-1})i[k]. \tag{23}$$

Here, z^{-1} is a delay and $P_c^n(z^{-1})$ is a nth-order polynomial in z^{-1} with coefficients c_k, e.g.,

$$P_a^2(z^{-1}) = a_0 + a_1 z^{-1} + a_2 z^{-2}. \tag{24}$$

Equation (23), modified to include a colored noise model,

$$P_a^2(z^{-1})(v_s[k] - v[k]) = P_b^2(z^{-1})i[k] + P_c^4(z^{-1})e[k] \tag{25}$$

was fit using preprocessed data with the ARMAX procedure in Matlab.

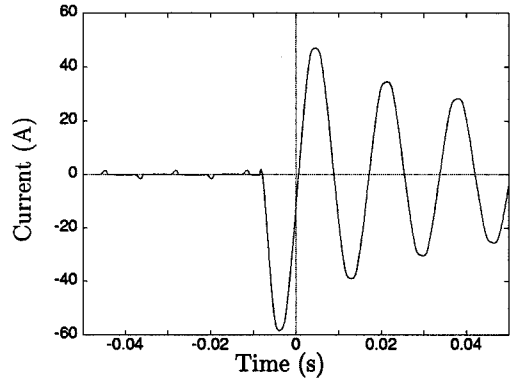

(a)

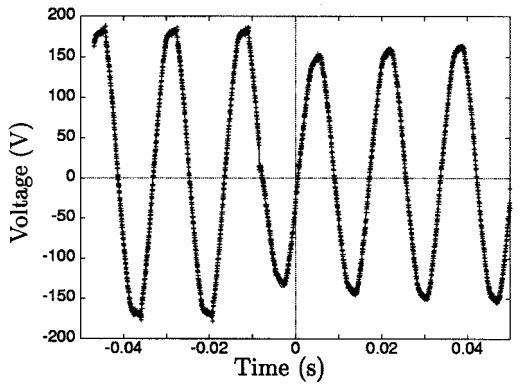

(b)

Fig. 5. (a) Measured current and (b) measured and predicted voltage for a laser printer using method A.

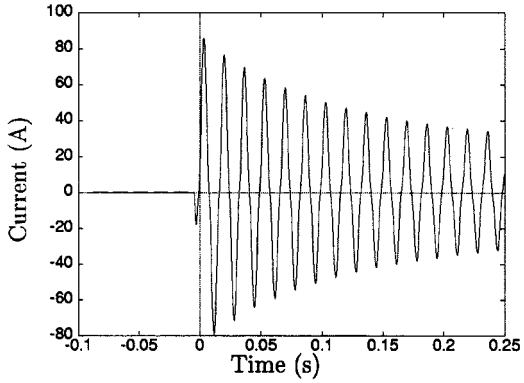

(a)

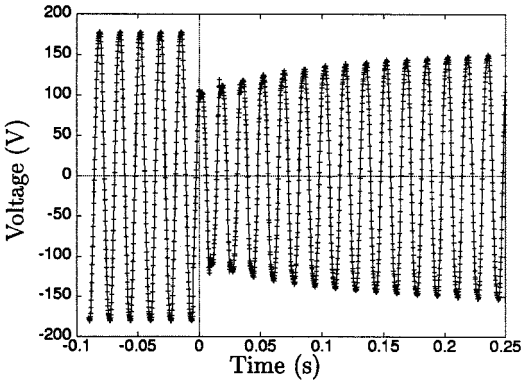

(b)

Fig. 6. (a) Measured current and (b) measured and predicted voltage for a vacuum cleaner using method A.

C. Voltage Prediction

Voltage distortion prediction using the discrete-time model involves iterating the difference equation (25) with the identified coefficient vectors a, b, and the measured or known current i. Preprocessing is not necessary in the prediction step, since the system identified with the preprocessed data is the same as the system acting on raw data.

VI. Experimental Results

A. Method A

A single-phase 1-kVA isolation transformer connected to a 60-Hz 30-A service was used to validate the hardware and software for method A. A relatively small transformer was chosen so that it could be removed from service and characterized independently during development. Using the test hardware, parameters R_0, δ, and L were determined. Finally, several realistic loads were connected to the transformer, and the method was tested by comparison of measured and predicted voltage waveform distortion.

1) Frequency Dependence of R: Fig. 4 shows estimated resistance $\hat{R}$ as a function of transient frequency f (Hz). The solid line is the interpolation of the data according to the model (17), and the dashed line shows the extrapolation of the model to lower frequencies. The estimated inductance $\hat{L}$ was 1.10 mH. Note that data were not available at lower frequencies because the capacitor values and currents needed for low-frequency tests would be excessive.

2) Voltage Prediction: Loads used to test the power quality prediction capabilities of the system included a laser printer and a vacuum cleaner. The results are shown in Figs. 5 and 6. Figs. 5(a) and 6(a) show measured current. Figs. 5(b) and 6(b) compare measured voltage (solid lines) and predicted voltage.

B. Method B

Method B was tested by connection to a standard single-phase 60-Hz 20-A 120-Vac outlet in the laboratory. No intermediate isolation transformer was used; method B was tested as it might be used in the field. The current source was driven with a series of windowed sine waves synthesized by a Sony/Tektronix AWG 2005 arbitrary waveform generator. Test signals were specified to the AWG 2005 as a series of samples, e.g.,

$$i_t[k] = A w_H[k](1 + \sin(kT_s\omega_t)) \tag{26}$$

where w_H is a Hanning window [4], T_s is the sampling period, and A is the amplitude of the test signal. Using this excitation, parameters of the discrete-time model were obtained as described in Section V, and predicted and measured voltage distortion were compared for a vacuum cleaner and laser printer

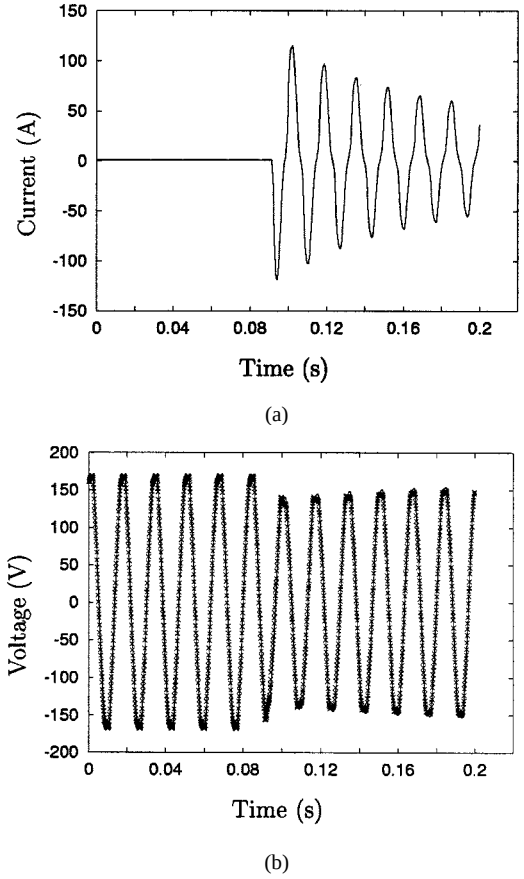

Fig. 7. (a) Measured current and (b) measured and predicted voltage for a vacuum cleaner using method B.

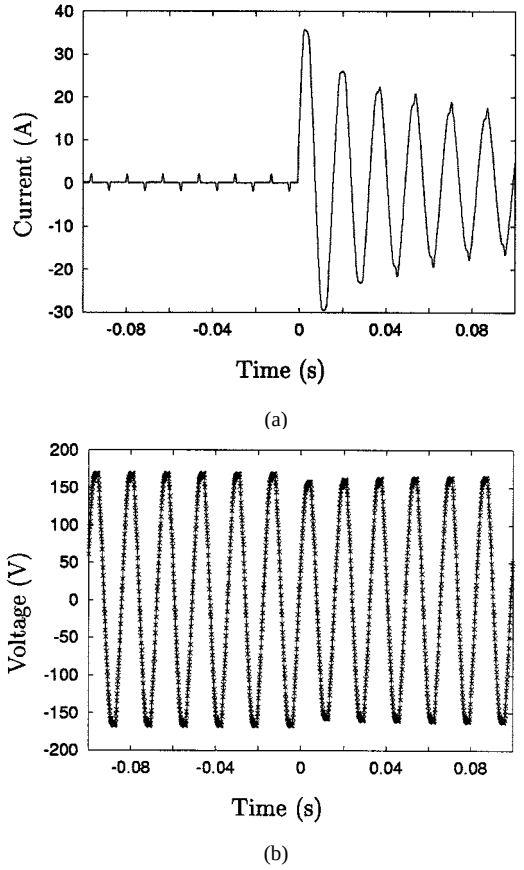

Fig. 8. (a) Measured current and (b) measured and predicted voltage for a laser printer using method B.

(see Figs. 7 and 8). The loads used are different from those used to test method A, but the transients are similar.

VII. Conclusions and Observations

The methods given in this paper characterize the point of load voltage distortion characteristics of a utility with simple, practical models. This information can be used for a variety of applications by utilities, and also commercial and industrial facilities managers. We anticipate that a one-time characterization of a building could be used with a library of nominal current waveforms to estimate voltage distortion in the building under different load conditions. This approach would produce good approximations as long as the distortion remained mild enough that "nominal" current profiles continued to be accurate. With more severe distortion, load-to-load interaction and more sophisticated load modeling would have to be considered.

In [3], the capability of the nonintrusive load monitor to determine the operating schedule of individual loads given access only to the aggregate current waveforms at the service entry was demonstrated. With additional knowledge collected during a one-time (or at least infrequent) examination of the details of a building's wiring, the location of loads with respect to the wiring, and the service connection impedances as determined by the techniques in this paper, the nonintrusive load monitor could provide continuous prediction of the local voltage waveforms at points of interest.

Acknowledgment

The authors gratefully acknowledge the valuable advice and support of T. Respress, D. K. Jackson, Prof. J. L. Kirtley, Jr., Prof. G. Verghese, Prof. B. Lesieutre, and Prof. L. Norford and Dr. C. Searles, Dr. D. Charvonia, and Dr. D. Cress. Comments of the reviewers were extremely thoughtful and led to substantial improvements. Essential hardware for this project was made available through a generous donation from the Intel Corporation. Test and measurement equipment were generously supplied by Tektronix and Hewlett-Packard.

References

[1] W. C. Beattie and S. R. Matthews, "Impedance measurement on distribution networks," in *Proc. 29th Universities Power Engineering Conf.*, Sept. 1994, pp. 117–120.

[2] S. R. Shaw, R. F. Lepard, and S. B. Leeb, "DESIRE: A power quality prediction system," in *Proc. 28th North American Power Symp.*, Nov. 1996, pp. 581–587.

[3] S. B. Leeb, S. R. Shaw, and J. L. Kirtley Jr., "Transient event detection in spectral envelope estimates for nonintrusive load monitoring," *IEEE Trans. Power Delivery*, vol. 10, pp. 1200–1210, July 1995.

[4] A. V. Oppenheim and R. W. Schafer, *Discrete-Time Signal Processing*. Englewood Cliffs, NJ: Prentice-Hall, 1989, pp. 444–464.

[5] A. V. Oppenheim and A. S. Willsky, *Signals and Systems*. Englewood Cliffs, NJ: Prentice-Hall, 1983, pp. 665–667.

[6] S. B. Leeb and J. L. Kirtley Jr., "A transient event detector for nonintrusive load monitoring," U.S. Patent 5 483 153, Jan. 9, 1996.

[7] G. R. Slemon, *Magnetoelectric Devices: Transducers, Transformers, and Machines*,. New York: Wiley, 1966.

[8] R. Johansson, *System Modeling and Identification*. Englewood Cliffs, NJ: Prentice-Hall, 1993, pp. 283–293.

[9] R. A. Bozorth, *Ferromagnetism*. Princeton, NJ: Van Nostrand, 1959, pp. 774–778.

Steven R. Shaw (S'97) received the B.S. degree in electrical engineering and the M.E. degree from Massachusetts Institute of Technology, Cambridge, in 1995 and 1997, respectively.

He is currently a Post-Doctoral Research Assistant in the Laboratory for Electromagnetic and Electronic Systems, Massachusetts Institute of Technology.

Chris Laughman received the B.S. degree in 1999 from the Laboratory of Electromagnetic and Electronic Systems, Massachusetts Institute of Technology, Cambridge, where he is currently working toward the M. Eng. degree.

Steven B. Leeb (S'89–M'91) received the B.S., M.S., E.E., and Ph.D. degrees from Massachusetts Institute of Technology, Cambridge, in 1987, 1989, 1990, and 1993, respectively.

Since 1993, he has been a member of the faculty in the Department of Electrical Engineering and Computer Science, Massachusetts Institute of Technology. He currently serves as the Carl Richard Soderberg Associate Professor of Power Engineering in the Laboratory for Electromagnetic and Electronic Systems. He is concerned with the design, analysis, development, and maintenance processes for all kinds of machinery with electrical actuators, sensors, or power electronic drives.

Dr. Leeb is a member of the IEEE Power Engineering Society, a Fellow of the Leaders for Manufacturing Program, Massachusetts Institute of Technology, and a member of Tau Beta Pi and Eta Kappa Nu.

Rob F. Lepard received the B.S. and M.E. degrees in electrical engineering from Massachusetts Institute of Technology, Cambridge, in 1996.

He is currently serving in the U.S. Air Force as a Second Lieutenant in the Aeronautical Systems Command, Wright-Patterson Air Force Base, Dayton, OH.